

A Wireless Servo Motor Drive with Bidirectional Motion Capability

Chaoqiang Jiang, *Student Member, IEEE*, K. T. Chau, *Fellow, IEEE*, Christopher H. T. Lee, *Senior Member, IEEE*, Wei Han, *Student Member, IEEE*, Wei Liu, *Student Member, IEEE*, and W. H. Lam, *Senior Member, IEEE*

Abstract- In this paper, a novel wireless servo motor drive is proposed and implemented, which artfully integrates wireless power transfer into the DC servo motor drive to achieve wireless bidirectional servo motion. Prominently, there is no power converter or controller at the servo motor side to realize the bidirectional rotation, while the motor control is fully conducted at the transmitter side. The key is to adopt only one transmitter with LCL network to achieve power equalization of two receiver coils, hence realizing bidirectional motion. Meanwhile, the phase-shift control method is newly developed to perform the desired speed control at the transmitter side, without requiring any switched capacitor arrays. As a result, the proposed wireless bidirectional servo motor drive takes the definite advantages of electrocution free and totally sealable. Both calculation and experimental results are presented to validate the feasibility and controllability. For the prototype, the transmission distance can reach up to 130 mm and the transmission efficiency can be up to 85%.

Index Terms- Wireless power transfer, wireless motor, bidirectional motor, servo motor, DC servo

I. INTRODUCTION

MORE than one hundred years ago, the concept of electrical energy transmission without wires was proposed by Nikola Tesla [1]. Currently, as one of the most epoch-making techniques, wireless power transfer (WPT) has been involved in various applications, especially for the electric-driven devices [2-5]. By utilizing this emerging technique, the energy receptor can harness wireless power from electromagnetic field in air and thus charge their battery in dynamic states or extreme operation conditions [6-7]. Since the WPT technique possesses the advantages of reliability, automation, safety, low maintenance, convenience, and

electrical isolation [8], more and more academic researchers and industries are getting involved in this emerging area. Thus, the WPT shows significant meanings for charging portable electronic devices [9], implanted medical devices [10], and electric vehicles [11-13].

Among so many WPT applications, the WPT for motor drive has been little researched. This is because the conventional WPT just changed the power delivery method, and the controller and converters are still needed at the motor side. Previously, a wireless in-wheel motor system was presented [14], which could alleviate the problem of conventional in-wheel motors for electric vehicles [15]. However, this is not a real wireless motor, which is actually a combination of the wireless battery charging system and the cable powered motor system. Besides, this kind of pseudo-wireless motors suffers from using additional controller and converters, which are bulky, lossy and costly. Consequently, a real wireless separately excited DC motor drive was proposed [16]. In this topology, only one transmitter is needed to wirelessly feed both the armature and field windings and there is no power converter at the motor side. However, this wireless DC motor drive could only provide unidirectional currents, hence resulting in unidirectional motion.

Generally, a multiple-receiver WPT system is used to power several ubiquitously existent devices or to extend the transmission distance [17-19]. For most multiple-receiver applications, the WPT system mainly focuses on transferring wireless power simultaneously to all receivers. However, for wireless motor drive applications, only one receiver needs to be energized among several receivers. Thus, a multiple-frequency WPT is needed to targetedly deliver power to the targeted phase winding [20]. By utilizing multiple resonant frequencies, the WPT system can also realize energy security [21]. Namely, the receivers with the same resonant frequency can pick up the wireless energy, while other receivers with different resonant frequencies can pick up nearly no energy.

Due to the high controllability and fast response, the DC servo motor has been widely used for control application. By artfully incorporating WPT into the servo motor, the wireless servo motor drive can possess the definite advantages of electrocution free and totally sealable while offering bidirectional servo motion.

Manuscript received November 22, 2018; revised January 09, 2019; accepted March 07, 2019. This work was supported by a grant (Project No. 17204317) from the Hong Kong Research Grants Council, Hong Kong Special Administrative Region, China. (Corresponding author: K. T. Chau, ktchau@eee.hku.hk.)

Chaoqiang Jiang, K. T. Chau, Wei Han, Wei Liu, and W. H. Lam are with Department of Electrical and Electronic Engineering, The University of Hong Kong, Hong Kong, China. (emails: cqjiang@eee.hku.hk, ktchau@eee.hku.hk, weihan@eee.hku.hk, liuweiliu@eee.hku.hk, whlam@eee.hku.hk).

Christopher H. T. Lee is with the School of Electrical and Electronic Engineering, Nanyang Technological University, Singapore. (email: chtlee@ntu.edu.sg)

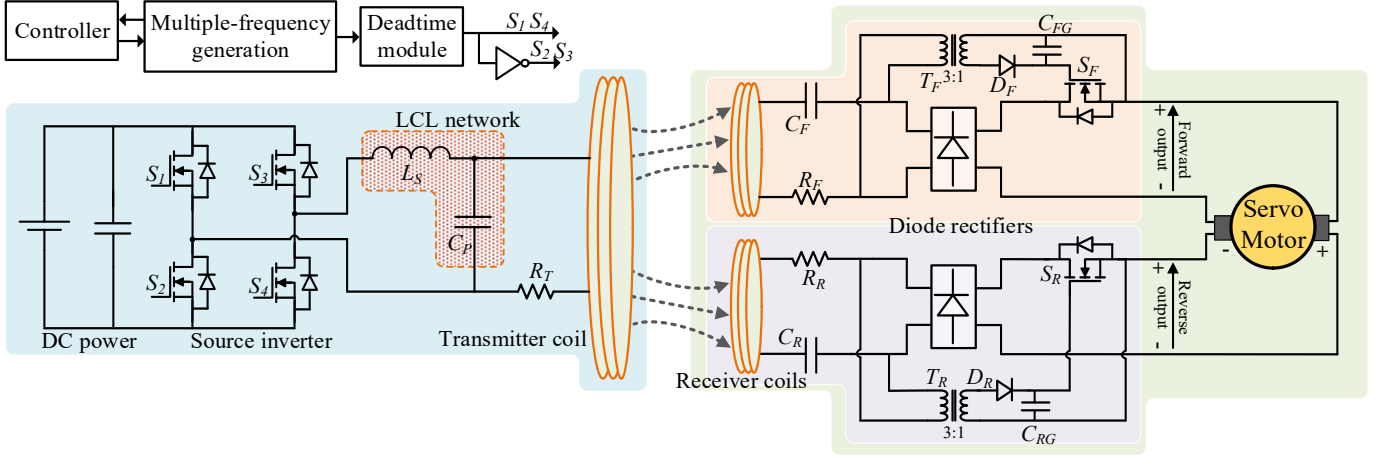


Fig. 1. Proposed system configuration of LCL wireless bidirectional servo motor drive.

In this paper, a novel wireless bidirectional servo motor drive is proposed and implemented. The main contributions of this paper are listed as follows. First, the selective multiple-frequency WPT is realized by incorporating the LCL network, instead of using the bulky switched-capacitor array. Second, the power equalization for the two motor motions is achieved at different operating frequencies. Besides, only one transmitter is required to feed the receiver for the servo motor. In order to create bidirectional motion, a self-drive circuit is coupled with each coil of the receiver to produce bipolar voltage across the servo motor and hence to achieve bidirectional operation. As a result, there will be no additional power supply or controller at the motor side. Meanwhile, the servo motion can be fully controlled by the transmitter, which is highly desirable for some practical applications such as a wireless rotatable table inside the glovebox.

In Section II, the system design and analysis of the proposed wireless bidirectional servo motor drive including the multi-frequency WPT and different compensations will be discussed. In Section III, the bidirectional control circuit and operation will be discussed. Then, in Section IV, an experimental prototype will be constructed and tested so as to verify the feasibility of the proposed system. Finally, a conclusion will be drawn in Section V.

II. MULTIPLE-FREQUENCY WPT

The proposed wireless bidirectional servo motor drive is shown in Fig. 1, which involves two main parts: the primary and the secondary. The primary part consists of a high frequency AC inverter, an LCL network, and one transmitter coil, which is operated at two different frequencies. Particularly, these two operating frequencies correspond to the two resonant frequencies of the series connected LC tanks in the secondary part. The secondary part consists of a receiver with two coils having different series connected compensation capacitors, two simple diode rectifiers, two pulse transformers, two MOSFETs for direction selection, and a permanent-

magnet DC servo motor. The upper receiver coil is used to drive the motor in the forward direction, whereas the lower receiver coil is for the reverse direction.

As shown in Fig. 1, the LCL network aims to provide multiple-frequency operation with only one transmitter. Since the two receiver LC tanks are with different resonant frequencies, each receiver LC tank can be separately excited and thus provide DC power to the motor based on the principle of selective WPT. When the operating frequency is set at the resonant frequency of the upper receiver, the upper receiver will pick up wireless power while the lower receiver will pick up nearly no energy, and thus the upper MOSFET S_F will be turned on while the lower MOSFET S_R will be turned off through the pulse transformers. Thus, the motor can be fed by a positive voltage, hence achieving forward motion. Due to the cross connection of the two DC outputs, namely the forward output and reverse output, the motor can be fed with bipolar voltages to achieve bidirectional motion. It should be noted that there is no additional battery or controller in the secondary part so that the wireless servo motor drive can be totally sealed.

The proposed system equivalent circuit is shown in Fig. 2 (a), where the inverter output is regarded as AC power source V_S ; L_S , L_T and R_T are the inductances of the series inductor and the transmitter coil, and the transmitter coil resistance, respectively; C_P is the capacitance of the parallel capacitor; I_S and I_T are the currents of the AC power source and the transmitter coil; L_b , C_b , R_b , I_b , U_i ($i=F, R$) are the inductances of receiver coils, the capacitances of the series compensated capacitor, the resistances of receiver coils, the currents, and the rectifier input voltages; M_{Ti} are the mutual inductance between the transmitter and receiver coils; M_{FR} is the mutual inductance between two receiver coils, which is neglected due to the same planar layout; U_M , I_M are the motor supplied voltage, and current; $R_M(n)$ is the equivalent resistance of the motor, which is related to the motor speed and load torque.

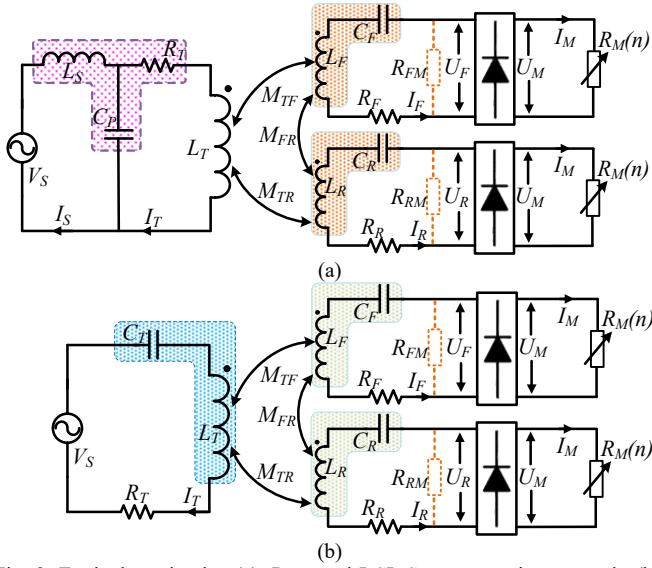


Fig. 2. Equivalent circuits. (a). Proposed LCL-S compensation network. (b). Conventional S-S compensation network.

A. Selectability of WPT

In this wireless servo motor drive system, one receiver coil with LC tank should be targeted while another one would not be targeted, and vice versa. For these two LC tanks with different resonant frequencies of f_F and f_R , they behave like two bandpass filters. And the corresponding angular frequencies ω_F , ω_R can be expressed as

$$\begin{cases} \omega_F = 2\pi f_F = 1/\sqrt{L_F C_F} \\ \omega_R = 2\pi f_R = 1/\sqrt{L_R C_R} \end{cases} \quad (1)$$

Particularly, when only one operating frequency ω is adopted at the transmitter, the currents I_F , I_R of the two receiver coils can be calculated by

$$I_F(\omega) = \frac{\omega M_{TF} I_T}{\sqrt{(R_F + R_{FM})^2 + (\omega L_F - \frac{1}{\omega C_F})^2}} \quad (2)$$

$$= \frac{M_{TF} I_T}{L_F \sqrt{\frac{\omega_F^2}{\omega^2 Q_F^2} + (1 - \frac{\omega_F^2}{\omega^2})^2}}$$

$$I_R(\omega) = \frac{M_{TR} I_T}{L_R \sqrt{\frac{\omega_R^2}{\omega^2 Q_R^2} + (1 - \frac{\omega_R^2}{\omega^2})^2}} \quad (3)$$

where $Q_i = \omega_i L_i / (R_i + R_{iM})$ ($i = F, R$) represents the Q-factor of each coil, and the R_{iM} is the converted equivalent resistance before the diode rectifier, which can be expressed as

$$R_{iM} = \frac{U_i}{I_i} = \frac{\delta}{\pi^2} \frac{U_M}{I_M} = \frac{\delta}{\pi^2} R_M(n) \quad (4)$$

For the servo motor, the operation current I_M can be determined by the electromagnetic torque T_{EM} , which can be calculated by

$$I_M = \frac{T_{EM}}{C_T \Phi} \quad (5)$$

where C_T is the torque constant, Φ is the air-gap flux per pole. Generally, the back electromotive force (EMF) E_M of a servo motor can be expressed as

$$E_M = C_e \Phi n \quad (6)$$

where C_e is the back EMF constant, n is the motor speed. Thus, the motor voltage equation can be expressed as

$$U_M = E_M + I_M R_a \quad (7)$$

where R_a is the armature winding resistance.

Based on (5)-(7), the motor equivalent resistance can be calculated at different torques and speeds. The system parameters are listed in TABLE I. When the torque is at the constant value of 10 Ncm, the $R_M(n)$ at the motor speeds of 500 rpm, 1000 rpm, and 1500 rpm can be calculated as 10.7 Ω , 20.5 Ω , and 30.3 Ω , respectively. Then the currents of the two coils with respect to different operating frequencies can be calculated as plotted in Fig. 3. The resonant frequencies of the forward and reverse LC tanks are set to 130 kHz and 160 kHz. It can be observed that the power flow path can be governed by the transmitter operating frequency. In other words, only the forward coil can pick up the wireless power when the transmitter is operated at f_F , while the reverse coil picks up nearly no power, and vice versa. Furthermore, it should be noted that the power variation will be created by this multiple-frequency WPT due to the different reflected impedances. In order to make sure that the forward and reverse rotations are under the same operating condition, the power equalization should be realized.

TABLE I SYSTEM PARAMETERS

Item	Value	Unit
Resonant frequencies (f_F, f_R)	130, 160	kHz
Resistance of transmitter coil (R_T)	0.6	Ω
Resistance of receiver coils (R_F, R_R)	0.3	Ω
Resistance of motor winding (R_a)	0.9	Ω
Mutual inductance (M_{TF}, M_{TR})	70	μ H
Inductance of transmitter coil (L_T)	0.71	mH
Inductance of receiver coil (L_F, L_R)	0.50	mH
LCL inductor (L_S)	0.213	mH
LCL compensated capacitor (C_P)	7.05	nF
Torque constant ($C_T \Phi$)	13.8	Ncm/A
Voltage constant ($C_e \Phi$)	14.2	V/krpm

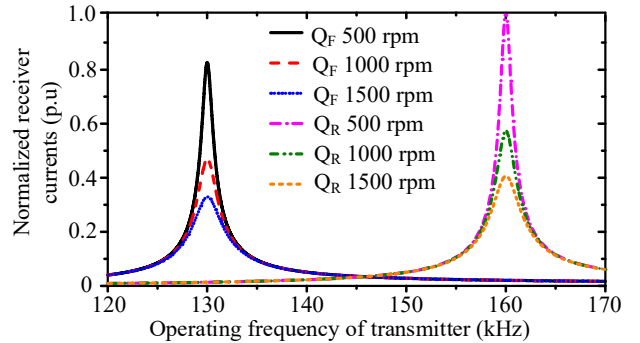


Fig. 3. Receiver current variations with respect to different operating frequencies of transmitter.

B. S-S Topology without Switched-capacitor Array

Generally, the operating frequency of the transmitter should be kept the same as the receiver LC tank's resonant frequency. For a multiple-frequency WPT system, a switched-capacitor array is usually required to discretely adjust the matched capacitance in accordance with the resonant frequency of the transmitter. However, this topology suffers from the drawbacks of higher switching stress and lower regulation flexibility. Thus, a series-to-series (S-S) topology without the switched-capacitor array was proposed to make the targeted receiver be operable under different resonant frequencies [22]. As shown in Fig. 2 (b), the forward and reverse receiver coil impedances are given by

$$\begin{cases} Z_F = j\omega L_F + \frac{1}{j\omega C_F} + R_F + R_{FM} \\ Z_R = j\omega L_R + \frac{1}{j\omega C_R} + R_R + R_{RM} \end{cases} \quad (8)$$

For the transmitter side, the total reflected impedance Z_{REF} can be expressed as

$$Z_{REF} = \frac{\omega^2 M_{TF}^2}{Z_F} + \frac{\omega^2 M_{TR}^2}{Z_R} \quad (9)$$

Thus, the S-S WPT system without the switched-capacitor array can be expressed as

$$\begin{bmatrix} j\omega L_T + \frac{1}{j\omega C_T} + R_T & j\omega M_{TF} & j\omega M_{TR} \\ j\omega M_{TF} & Z_F & j\omega M_{FR} \\ j\omega M_{TR} & j\omega M_{FR} & Z_R \end{bmatrix} \cdot \begin{bmatrix} I_T \\ I_F \\ I_R \end{bmatrix} = \begin{bmatrix} V_s \\ 0 \\ 0 \end{bmatrix} \quad (10)$$

And the transmitter current at different operating frequencies can be calculated as

$$I_T = \frac{V_s}{j\omega L_T + \frac{1}{j\omega C_T} + R_T + Z_{REF}} \quad (11)$$

On the other hand, according to (2) and (3), the receiver currents of I_F and I_R can be calculated and then the received power P_i for the motor can be expressed as

$$P_i = I_i^2 R_{iM} \quad (i = F, R) \quad (12)$$

In this wireless bidirectional servo motor drive, the operating frequency of the transmitter is always kept at 130 kHz or 160 kHz, which are corresponding to the two receiver coil resonant frequencies. When the torque is kept at 10 Ncm and the speed is 1000 rpm, the received power of the S-S topology with respect to different resonant frequencies of the $L_T C_T$ tank is shown in Fig. 4. It can be observed that when the resonant frequency of the $L_T C_T$ tank is selected at 148 kHz, namely, C_T equals 1.63 nF, the two coils can independently receive the same power under the two different operating frequencies of the transmitter. Thus, power equalization between the forward motion and the reverse motion can be achieved when the transmitter resonant frequency is set to 148 kHz. Actually, the resonant frequencies of the two receiver LC tanks are set at 130 kHz and 160 kHz so that the operating frequency of the transmitter is always kept at 130 kHz or 160

kHz, depending on the selection of motion. Although the power equalization can be fulfilled, a high voltage-to-current rating is needed for the transmitter.

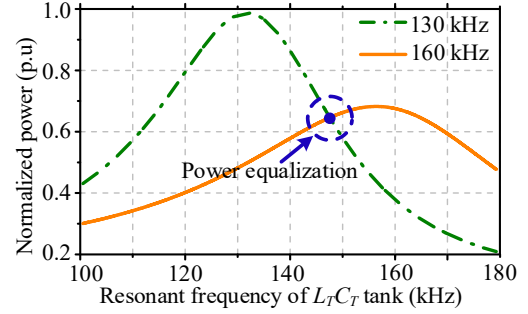


Fig. 4. Received power for S-S topology with respect to resonant frequency of $L_T C_T$ tank.

C. LCL-S Topology without Switched-capacitor Array

Recently, the LCL network has been developed for electric vehicle charging, soft-switching WPT, as well as resonant frequency irrelevance of coupling coefficient and load condition [23-25]. However, the LCL multiple-frequency WPT system is absent in literature. In this wireless servo motor drive, the LCL network is adopted to achieve the desired power equalization of the servo motor with bidirectional motion. As shown in Fig. 2 (a), one more inductor is added when comparing to the S-S topology.

Considering the reflected impedance from the receiver, the primary impedance Z_S can be expressed as

$$Z_S = j\omega L_S + \frac{1}{j\omega C_p} \parallel (j\omega L_T + R_T + Z_{REF}) \quad (13)$$

Then the LCL network WPT system model can be expressed as

$$\begin{bmatrix} Z_S & 0 & 0 \\ j\omega M_{TF} & Z_F & j\omega M_{FR} \\ j\omega M_{TR} & j\omega M_{FR} & Z_R \end{bmatrix} \cdot \begin{bmatrix} I_T \\ I_F \\ I_R \end{bmatrix} = \begin{bmatrix} V_s \\ 0 \\ 0 \end{bmatrix} \quad (14)$$

Based on the system model, the transmitter coil current I_T can be calculated by

$$I_T = \frac{V_s}{j\omega L_T + R_T + Z_{REF}} \left(1 - \frac{j\omega L_S}{Z_S}\right) \quad (15)$$

Hence, the targeted receiver power can be deduced by using (2), (3) and (12). Due to the additional L_S in the primary, the parameter design is the key point to achieve the power equalization. In general, the transmitter coil inductance is firstly determined. Then the inductor L_S , and capacitor C_p will be determined once the parameters fulfill the power equalization, which are defined as

$$L_S = k \cdot L_T \quad (16)$$

$$\omega_{L_S C_p} = \frac{1}{\sqrt{L_S C_p}} \quad (17)$$

where k is the inductance ratio, $\omega_{L_S C_p}$ is the resonant frequency of the $L_S C_p$ tank.

For the LCL-S topology, an additional $L_S C_p$ tank is included. The parameter calculations are governed by (15)-

(17). The received power distribution with respect to inductance ratio k and resonant frequency of the $L_S C_P$ tank is shown in Fig. 5. It can be observed that there is an intersection curve line between the received power distributions at the operating frequencies of 130 kHz and 160 kHz. This is a set of power equalization points. As shown in Fig. 5, a large inductance ratio k will cause less received power and increase the voltage-to-current rating of the inverter. Also, a small inductance ratio k will cause lower resonant frequency of the $L_S C_P$ tank and larger capacitance of C_P . Thus, k is selected as 0.3. When k equals 0.3, f_{CPLS} equals 71 kHz, namely, $L_S = 0.213$ mH and $C_P = 7.05$ nF, the received power of the servo motor can achieve power equalization during bidirectional motion.

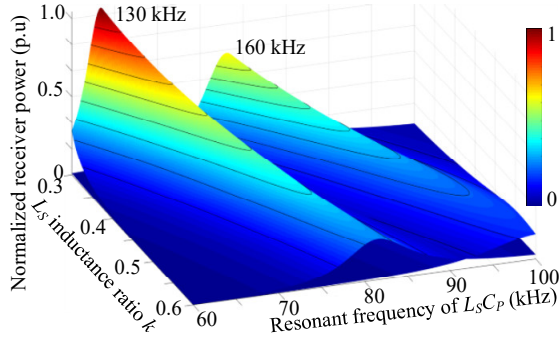


Fig. 5. Received power distribution with respect to inductance ratio k and resonant frequency of $L_S C_P$ tank.

D. Comparison between S-S and LCL-S Topologies

For a conventional multiple-frequency WPT system, a switched-capacitor array can be used to select different resonant frequencies. However, as shown in Fig. 6, the high frequency current through the capacitor will induce high voltage stress for the power switches. It can be found that the drain-source voltage can reach up to 1.6 kV when the transmitter changes the operating frequency from 160 kHz to 130 kHz at 0.8 A.

As aforementioned, both the S-S and LCL-S topologies can fulfill the power equalization at the two operating frequencies of 130 kHz and 160 kHz without using any switched-capacitor arrays. As shown in Fig. 7, the corresponding inverter output voltage and receiver coil current waveforms are simulated. In the S-S topology, when the operating frequency is set at 130 kHz, the forward receiver coil can pick up energy while there is nearly no current flowing in the reverse receiver coil, as shown in Fig 7 (a) and (b), as well as the LCL-S topology. It can be observed that the receiver current can be effectively controlled by the operating frequency and power equalization can be well achieved, no matter using S-S or LCL-S topology. However, it can be found that the S-S topology has the drawbacks of much higher DC supply voltage and hence voltage stress of power switches under the same received power when comparing to the LCL-S topology. Therefore, the LCL topology is adopted in the proposed wireless servo motor drive.

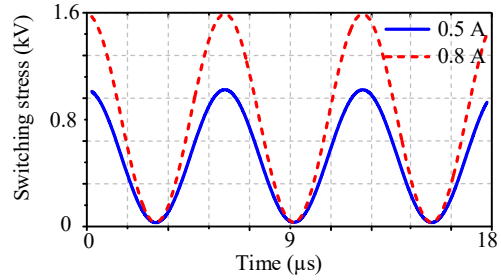


Fig. 6. Voltage stress of power switches when changing operating frequency from 160 kHz to 130 kHz.

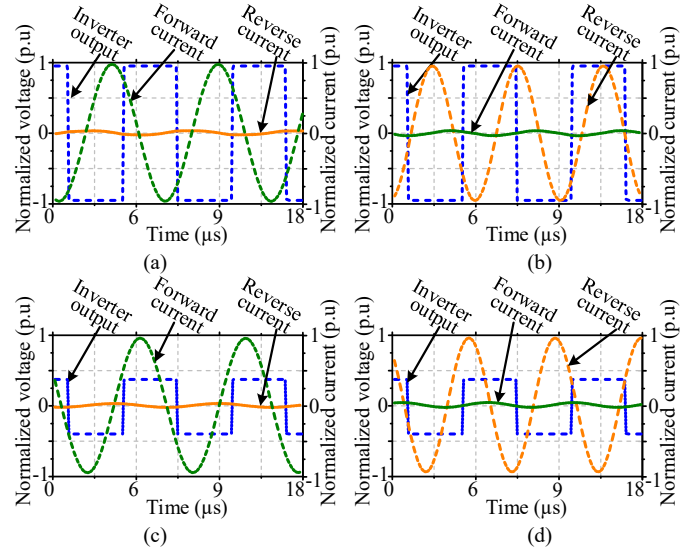


Fig. 7. Simulation waveforms of inverter output voltage and receiver coil currents. (a). 130 kHz operation of S-S topology. (b). 160 kHz operation of S-S topology. (c). 130 kHz operation of LCL-S topology. (d). 160 kHz operation of LCL-S topology.

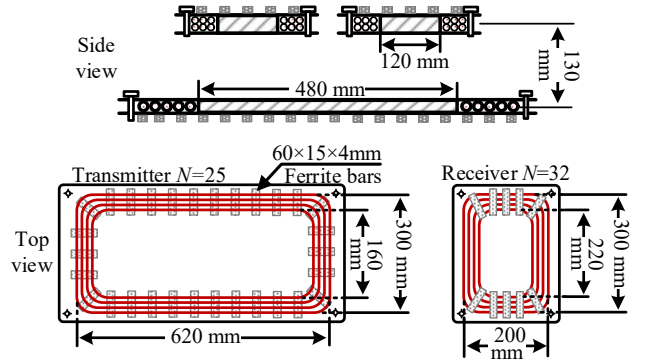


Fig. 8. Geometries of transmitter, receiver coils and ferrite bars.

III. BIDIRECTIONAL CIRCUIT AND OPERATION CONTROL

A. Finite Element Analysis

As shown in Fig. 8, only one transmitter is adopted to serve the two double-layer receiver coils. These three coils are all wound by Litz wire with the concentrated winding. In order to reduce the flux leakage and improve the transfer efficiency, several soft ferrite bars are laid at the bottom of the transmitter coil and at the top of the two receiver coils. Since the soft ferrite offers low coercivity, it can effectively enhance

magnetic fields with insignificant hysteresis and eddy current losses.

By using the finite element analysis (FEA) software JMAG, the magnetic field characteristics can be determined, hence assessing the proposed selectability. As shown in Fig. 9 (a) and (b), it can be observed that the magnetic flux lines can well focus on the targeted receiver coil. Besides, the magnetic flux density distributions are shown in Fig. 9 (c) and (d). It can be found that the magnetic flux density of the targeted forward coil is much higher than that of the untargeted reverse coil when the operating frequency of the transmitter is set at 130 kHz. Meanwhile, the magnetic flux density of the targeted reverse coil is much higher than that of the untargeted forward coil when the operating frequency of the transmitter is set at 160 kHz. These magnetic field distributions verify that the two receiver coils can be controlled independently by changing the transmitter operating frequency.

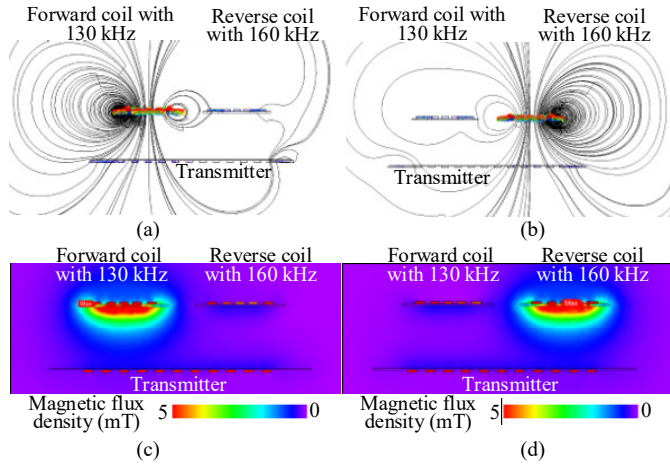


Fig. 9. Magnetic field distributions. (a). Flux line distribution at 130 kHz. (b). Flux line distribution at 160 kHz. (c). Flux density distribution at 130 kHz. (d). Flux density distribution at 160 kHz.

B. Bidirectional Circuit Analysis

For a conventional servo motor drive, bidirectional motion control can readily be achieved by using a power converter to feed bipolar DC currents into the motor. However, for the proposed wireless servo motor drive, it is undesirable to have an additional power converter to feed the motor at the receiver side. Although the use of multi-frequency WPT can provide bipolar DC currents at the two receiver coils, these currents cannot be directly fed into the motor due to the short-circuiting effect across the motor terminals as depicted in Fig. 10 (a) and (b).

A self-drive circuit is proposed, which is coupled with each receiver coil to solve the above short-circuiting problem. This self-drive circuit employs a pulse transformer to drive a MOSFET switch to maintain the current feeding into the motor. The principle of operation is described as follows:

- **Forward motion:** As shown in Fig. 11 (a) and (b), the forward receiver coil is activated to pick up wireless power at 130 kHz. Thus, the upper pulse transformer can drive the upper MOSFET to maintain turn-on while the

lower pulse transformer is idling. Thus, a positive current can be effectively fed into the motor to achieve forward rotation.

- **Reverse motion:** As shown in Fig. 11 (c) and (d), the reverse receiver coil is activated to pick up wireless power at 160 kHz. Thus, the lower pulse transformer can drive the lower MOSFET to maintain turn-on while the upper pulse transformer is idling. Thus, a negative current can be effectively fed into the motor to achieve reverse rotation.

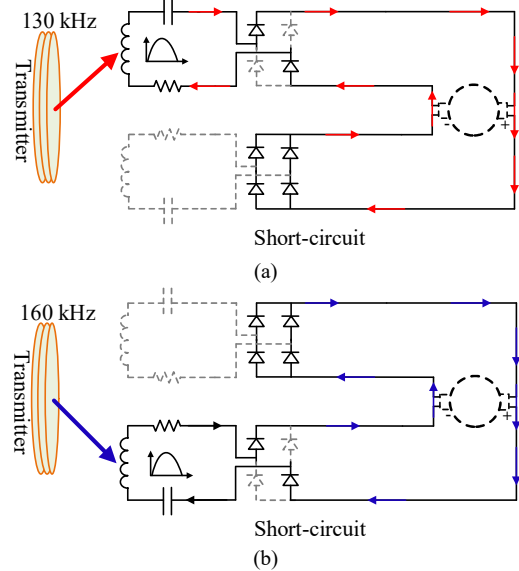
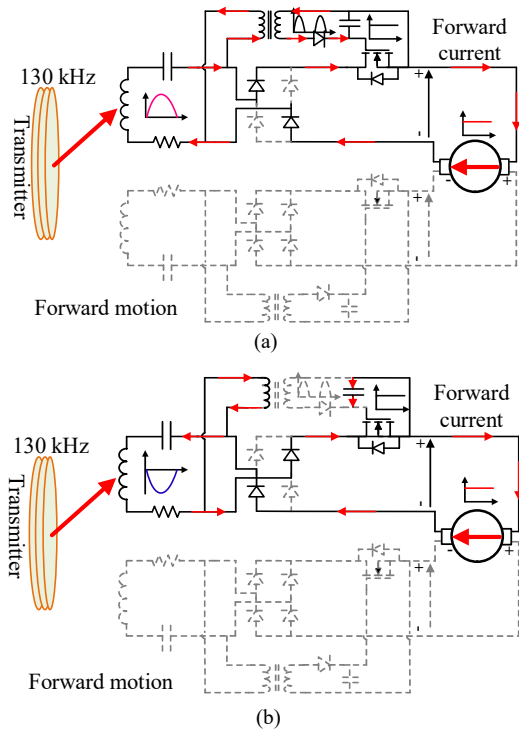


Fig. 10. Current flow paths without self-drive circuits. (a). 130 kHz. (b). 160 kHz.



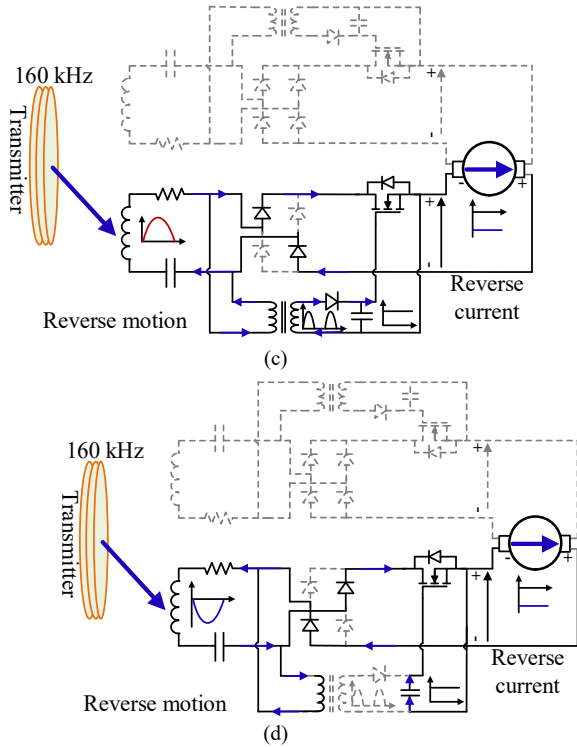


Fig. 11. Current flow paths with self-drive circuits. (a). Positive half-cycle at 130 kHz. (b). Negative half-cycle at 130 kHz. (c). Positive half-cycle at 160 kHz. (d). Negative half-cycle at 160 kHz.

Due to the servo motor's wide speed and torque ranges, the voltage/current range loaded into the self-drive circuit is also wide. For the M818 servo motor adopted in this paper, the rated speed, torque, voltage and current are 2000 rpm, 30 Ncm, 2.2 A, and 32 V, respectively. Thus, the voltage/current range loaded into the self-drive circuit will be from 15Ω to 50Ω . In order to improve the system selectability, the receiver coil inductance of 0.5 mH is adopted. As a result, the receiver resonant LC tank with 130 kHz will behave as an impedance of 170Ω at the operating frequency of 160 kHz, which is much larger than the motor voltage/current range. Considering the servo motor operation voltage and the threshold voltage of the MOSFET, the pulse transformer ratio is set at 3:1 to ensure that the self-drive circuit can properly drive the MOSFET in such a wide range of operation.

C. Speed Control Operation

The key contribution of the proposed wireless bidirectional servo motor drive is the elimination of bulky battery, converter, and controller at the receiver side. The control is carried out at the transmitter side. Due to the proposed LCL network for power equalization, the operating frequencies of the transmitter should be kept at the two resonant frequencies of the two LC tanks. In order to realize motor control while keeping the operating frequencies, the phase-shift control method is adopted at the transmitter side, which can offer the full operation range from 0° to 180° . As shown in Fig. 12, the phase-shift control method serves to adjust the phase shift

angle θ between the switch S_1 and the switch S_4 , namely controlling the charging time of the LCL network.

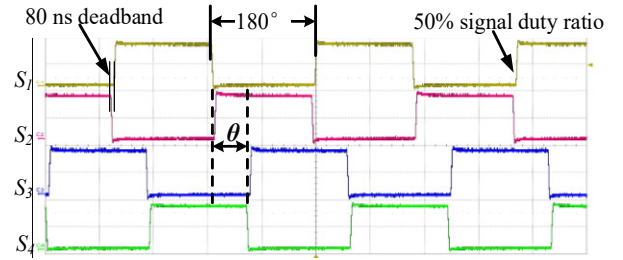


Fig. 12. Control signal waveforms of phase-shift control.

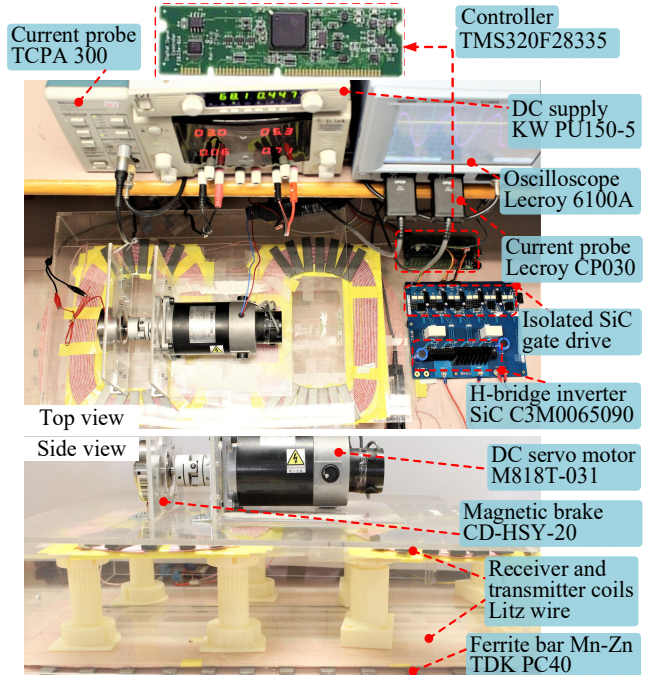


Fig. 13. Experimental setup of wireless bidirectional servo motor drive.

IV. EXPERIMENTAL VERIFICATION

Experiments have been carried out to verify the proposed wireless bidirectional servo motor drive. A setup is built as shown in Fig. 13 in which KENWOOD PU150-5 is used as the DC power supply for the H-bridge inverter with four SiC MOSFETs C3M0065090. The isolated SiC gate drive is realized by using 6N137, IR2128S, and ZDT6790. A deadband of 80 ns is adopted for the inverter to reduce the switching loss. The Lecroy 6100A, Lecroy CP030 and Tektronix TCPA300 are used to measure and display the current waveforms. In order to reduce the skin and proximity effects, the Litz wire (200×0.1 mm) is adopted for both the transmitter and receiver coils. The magnetic brake CD-HSY-20 is used as motor load. Practically, the operating frequencies f_T and f_R are set at 138 kHz and 169 kHz, respectively. Due to the difficulty in finding practical capacitors and inductors exactly equal to the calculated capacitances and inductances as well as the evitable tolerances of practical component values,

the practical operating frequencies are slightly different from the theoretical ones.

Firstly, the currents of the receiver forward and reverse coils, as well as the current of the servo motor are measured as shown in Fig. 14. It can be found that the motor current can be successfully controlled to achieve bidirectional motion by changing the operating frequency. When the transmitter operating frequency is set at 138 kHz, the current of the targeted forward receiver coil becomes 1.21 A and the corresponding motor current becomes 0.97 A, hence achieving forward rotation as shown in Fig. 14 (a). Meanwhile, the current of the nontargeted reverse receiver coil can pick up nearly zero current. On the other hand, when the transmitter operating frequency is set at 169 kHz, the current of the targeted reverse receiver coil becomes 1.26 A and the motor current becomes -1.02 A, hence achieving reverse rotation as shown in Fig. 14 (b). These results verify that the proposed system can effectively realize the bidirectional wireless motor drive and power equalization by utilizing the LCL network.

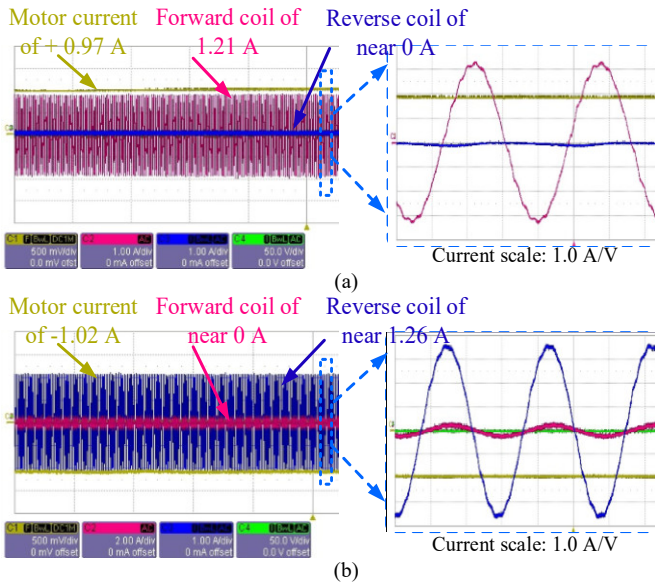


Fig. 14. Measured current waveforms with LCL topology. (a). Forward rotation with 138 kHz operation. (b). Reverse rotation with 169 kHz.

Secondly, in order to highlight the superiority of the LCL network, both LCL-S and S-S topologies are built for experimentation as shown in Fig. 15. The measured current and voltage waveforms of the S-S topology are shown in Fig. 15(a), and those of the LCL-S topology are shown in Fig. 15(b). It can be observed that the inverter output voltage of the S-S topology needs to be 96 V to achieve the motor current of -0.65 A, while the inverter output of the LCL-S topology is only 65 V to achieve the motor current of -0.66 A, which is much lower than that of the S-S topology. Thus, it verifies that the LCL-S compensation network can effectively reduce the requirement of DC supply voltage and also reduce the voltage stress of power switches when comparing to the S-S compensation network, which matches well with the simulation results.

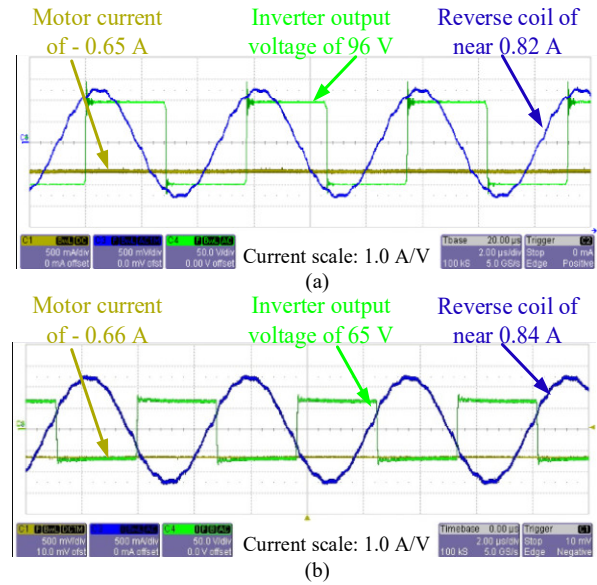


Fig. 15. Comparison between S-S and LCL-S topologies under the same motor current. (a). Waveforms of S-S topology. (b). Waveforms of LCL-S topology.

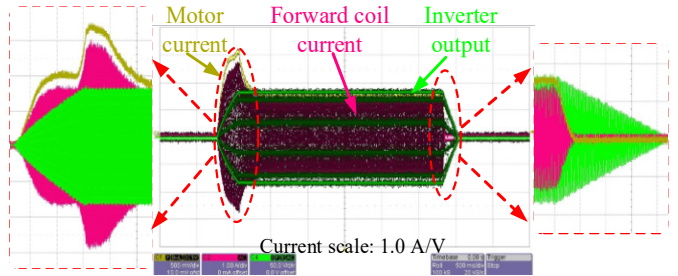


Fig. 16. Measured transient voltage and current responses during start and stop processes.

Thirdly, the motor transient responses during the start and stop processes are shown in Fig. 16. It can be observed that the proposed wireless motor can be effectively started and braked similar to a normal wired servo motor. Furthermore, the measured voltage and current waveforms at different phase-shift angles are shown in Fig. 17. As shown in Fig. 17 (a) and (b), the motor current can be effectively controlled by using phase-shift control, where the motor current is 0.82A at the phase-shift angle of 30° while the motor current is 0.68A at the phase-shift angle of 70° . Since the phase-shift control is to adjust the charging time for the primary LC tank, the wireless power transferred to the motor is smooth enough and there will be no obvious torque ripple. When the operating frequency is set at 169 kHz, the voltage and current waveforms of the motor and inverter are measured as shown in Fig. 18. Hence, it can deduce that the motor input voltage and current are 23.4 V and 0.72 A, respectively, while the inverter input voltage and current are 90 V and 0.22 A, respectively. Thus, the transmission efficiency from the DC power supply to the motor terminals can be calculated, which equals 85%.

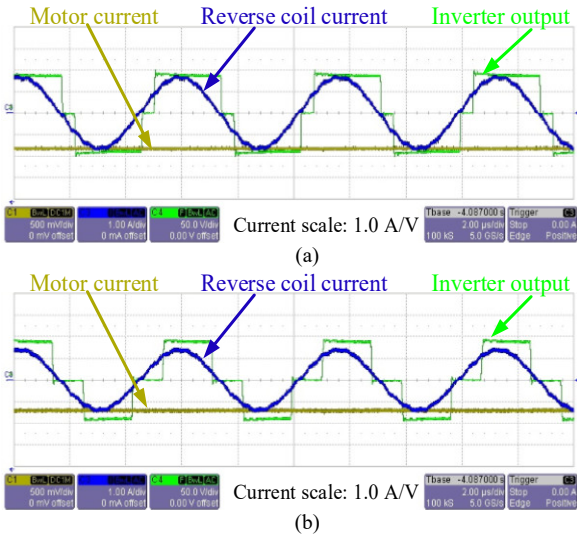


Fig. 17. Measured voltage and current waveforms at different phase-shift angles. (a). 30°. (b). 70°.

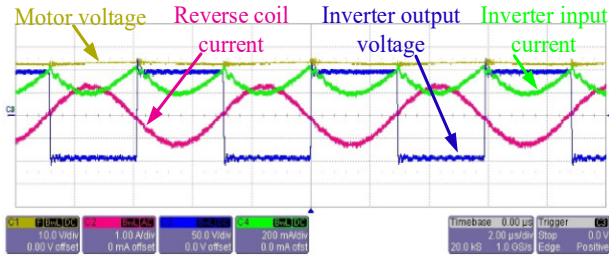


Fig. 18. Measured voltage and current waveforms of the motor and inverter when operating frequency is set at 169 kHz.

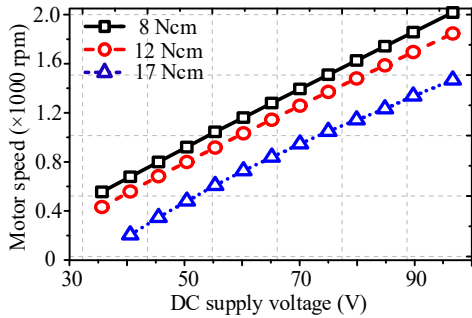


Fig. 19. Speed control for different load torques using DC supply voltage control.

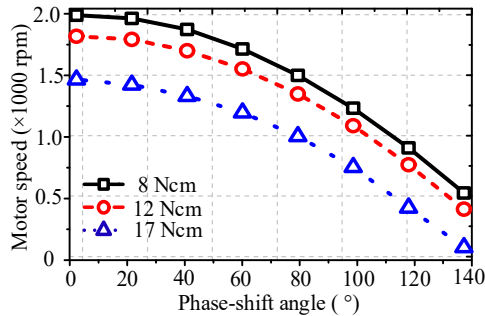


Fig. 20. Speed control for different load torques using phase-shift control.

Finally, to further validate the speed control of the proposed wireless servo motor drive, both the DC supply voltage control and the phase-shift control are implemented as shown in Fig. 19 and Fig. 20, respectively. It can be found that motor speed can be effectively controlled by the DC supply voltage for different load torques from 0 rpm to 2000 rpm. At the same time, it can be observed that the phase-shift method can provide smooth motor speed control for different load torques and the available phase-shift control range can vary from 0° to 140°. As a result, both the DC supply voltage control and phase-shift control can realize smooth motor speed control. However, the DC supply voltage control has the drawback of an additional DC-DC converter needed, while the phase-shift control only needs to regulate the pulse-width modulated (PWM) output of the H-bridge inverter. Therefore, the phase-shift control is more suitable for this wireless servo motor drive.

V. CONCLUSION

In this paper, a wireless bidirectional servo motor drive has been proposed and implemented, which takes the definite advantages of electrocution free and totally sealable. By newly adopting the LCL network, the switched-capacitor array for the multiple-frequency WPT can be eliminated and the two receiver coils can offer power equalization for bidirectional motion. Moreover, a self-drive circuit has been proposed to switch the rotation direction by only changing the operating frequency of the transmitter. Consequently, there is no converter, controller or battery at the motor side. Furthermore, the phase-shift control has been developed to perform effective servo motor control at the transmitter side. Both the simulation and experimental results have been provided to verify the proposed system. As a result, the system prototype can provide the transmission efficiency of 85% with the transmission distance of 130 mm.

REFERENCES

- [1] N. Tesla, "The transmission of electrical energy without wires," *Electrical World and Engineer*, Mar., 1904.
- [2] H. Hao, G. A. Covic, and J. T. Boys, "A parallel topology for inductive power transfer power supplies," *IEEE Transactions on Power Electronics*, vol. 29, no. 3, pp. 1140-1151, Mar., 2014.
- [3] J. Huh, S. W. Lee, W. Y. Lee, G. H. Cho, and C. T. Rim, "Narrow-width inductive power transfer system for online electrical vehicles," *IEEE Transactions on Power Electronics*, vol. 26, no. 12, pp. 3666-3679, Dec., 2011.
- [4] C. Jiang, K. T. Chau, Y. Leung, C. Liu, C. H. T. Lee, and W. Han, "Design and analysis of wireless ballastless fluorescent lighting," *IEEE Transactions on Industrial Electronics*, vol. 66, no. 5, pp. 4065-4074, May, 2019.
- [5] W. Han, K. T. Chau, and Z. Zhang, "Flexible induction heating using magnetic resonant coupling," *IEEE Transactions on Industrial Electronics*, vol. 64, no. 3, pp. 1982-1992, Mar., 2017.
- [6] C. Zhang, D. Lin, N. Tang, and S. Y. R. Hui, "A novel electric insulation string structure with high-voltage insulation and wireless power transfer capabilities," *IEEE Transactions on Power Electronics*, vol. 33, no. 1, pp. 87-96, Jan., 2018.
- [7] S. R. Cove, M. Ordóñez, N. Shafiee, and J. Zhu, "Improving wireless power transfer efficiency using hollow windings with track-width-ratio," *IEEE Transactions on Power Electronics*, vol. 31, no. 9, pp. 6524-6533, Nov., 2016.

- [8] M. Liu, M. Fu, and C. Ma, "Low-harmonic-contents and high-efficiency class E full-wave current-driven rectifier for megahertz wireless power transfer systems," *IEEE Transactions on Power Electronics*, vol. 32, no. 2, pp. 1198-1209, Apr., 2017.
- [9] A. P. Sample, D. T. Meyer, and J. R. Smith, "Analysis, experimental results, and range adaptation of magnetically coupled resonators for wireless power transfer," *IEEE Transactions on Industrial Electronics*, vol. 58, no. 2, pp. 544-554, Feb., 2011.
- [10] C. Liu, C. Jiang, J. Song, and K. T. Chau, "An effective sandwiched wireless power system for charging implantable cardiac pacemaker," *IEEE Transactions on Industrial Electronics*, vol. 66, no. 5, pp. 4108-4117, May, 2019.
- [11] S. Y. Choi, B. W. Gu, S. Y. Jeong, and C. T. Rim, "Advances in wireless power transfer systems for roadway-powered electric vehicles," *IEEE Journal of Emerging and Selected Topics in Power Electronics*, vol. 3, no. 1, pp. 18-36, Mar., 2015.
- [12] K. T. Chau, C. Jiang, W. Han, and C. H. T. Lee, "State-of-the-art electromagnetics research in electric and hybrid vehicles," *Progress In Electromagnetics Research*, vol. 159, pp. 139-157, Oct., 2017.
- [13] V. B. Vu, D. H. Tran, and W. Choi, "Implementation of the constant current and constant voltage charge of inductive power transfer systems with the double-sided LCC compensation topology for electric vehicle battery charge applications," *IEEE Transactions on Power Electronics*, vol. 33, no. 9, pp. 7398 - 7410, Sept., 2018.
- [14] M. Sato, G. Yamamoto, D. Gunji, T. Imura, and H. Fujimoto, "Development of wireless in-wheel motor using magnetic resonance coupling," *IEEE Transactions on Power Electronics*, vol. 31, no. 7, pp. 5270-5278, July, 2016.
- [15] K. T. Chau, *Electric Vehicle Machines and Drives: Design, Analysis and Application*: Wiley-IEEE Press, 2015.
- [16] C. Jiang, K. T. Chau, T. W. Ching, C. Liu, and W. Han, "Time-division multiplexing wireless power transfer for separately excited DC motor drives," *IEEE Transactions on Magnetics*, vol. 53, no. 11, pp. 8205405: 1-5, Nov., 2017.
- [17] A. Kurs, R. Moffatt, and M. Soljačić, "Simultaneous mid-range power transfer to multiple devices," *Applied Physics Letters*, vol. 96, no. 4, pp. 044102, Jan., 2010.
- [18] B. L. Cannon, J. F. Hoburg, D. D. Stancil, and S. C. Goldstein, "Magnetic resonant coupling as a potential means for wireless power transfer to multiple small receivers," *IEEE Transactions on Power Electronics*, vol. 24, no. 7, pp. 1819-1825, July, 2009.
- [19] S. Moon, and G. W. Moon, "Wireless power transfer system with an asymmetric four-coil resonator for electric vehicle battery chargers," *IEEE Transactions on Power Electronics*, vol. 31, no. 10, pp. 6844-6854, Dec., 2016.
- [20] Y. J. Kim, D. Ha, W. J. Chappell, and P. P. Irazoqui, "Selective wireless power transfer for smart power distribution in a miniature-sized multiple-receiver system," *IEEE Transactions on Industrial Electronics*, vol. 63, no. 3, pp. 1853-1862, Mar., 2016.
- [21] Z. Zhang, K. T. Chau, C. Qiu, and C. Liu, "Energy encryption for wireless power transfer," *IEEE Transactions on Power Electronics*, vol. 30, no. 9, pp. 5237-5246, Sept., 2015.
- [22] W. Liu, K. T. Chau, C. H. T. Lee, C. Jiang, and W. Han, "A switched-capacitorless energy-encrypted transmitter for roadway-charging electric vehicles," *IEEE Transactions on Magnetics*, vol. 54, no. 11, pp. 1-6, July, 2018.
- [23] C. S. Wang, G. A. Covic, and O. H. Stielau, "Investigating an LCL load resonant inverter for inductive power transfer applications," *IEEE Transactions on Power Electronics*, vol. 19, no. 4, pp. 995-1002, July, 2004.
- [24] L. Chen, S. Liu, Y. C. Zhou, and T. J. Cui, "An optimizable circuit structure for high-efficiency wireless power transfer," *IEEE Transactions on Industrial Electronics*, vol. 60, no. 1, pp. 339-349, Jan., 2013.
- [25] D. J. Thrimawithana, and U. K. Madawala, "A generalized steady-state model for bidirectional IPT systems," *IEEE Transactions on Power Electronics*, vol. 28, no. 10, pp. 4681-4689, Oct., 2013.



Chaoqiang Jiang (S'16) received the B.Eng. and M.Eng. degrees from the Department of Automation, Wuhan University, Wuhan, China, in 2012 and 2015, respectively. He is currently working toward the Ph.D. degree in the Department of Electrical and Electronic Engineering, The University of Hong Kong, Hong Kong, China.

His research interests include power electronics, wireless power transfer techniques, and electric vehicle technologies.



K. T. Chau (M'89–SM'04–F'13) received the B.Sc. (Eng.), M.Phil., and Ph.D. degrees in electrical and electronic engineering from The University of Hong Kong, Hong Kong, in 1988, 1991, and 1993, respectively.

Since 1995, he has been with The University of Hong Kong, where he is currently a Professor in the Department of Electrical and Electronic Engineering. He is the author of nine books and more than 300 journal papers. His research interests include electric and hybrid vehicles, power electronics and drives, and renewable energies.

Prof. Chau is a Fellow of the Institution of Engineering and Technology (IET), U.K., and of the Hong Kong Institution of Engineers (HKIE). He currently serves as a Coeditor of the *Journal of Asian Electric Vehicles*. He is a Chartered Engineer in Hong Kong. He received the Changjiang Chair Professorship from the Ministry of Education, China, and the Environmental Excellence in Transportation Award for Education, Training, and Public Awareness from the Society of Automotive Engineers (SAE) International.



Christopher H. T. Lee (M'12–SM'18) received the B.Eng. (First Class Honours) degree, and Ph.D. degree both in electrical engineering from Department of Electrical and Electronic Engineering, The University of Hong Kong, Hong Kong.

He currently serves as an Assistant Professor in Nanyang Technological University, a Visiting Assistant Professor in Massachusetts Institute of Technology, an Honorary Assistant Professor in the alma mater. His research interests are Electric Machines and Drives, Renewable Energies, and Electric Vehicle Technologies. In these areas, he has published 1 book, 3 book chapters, and about 70 referred papers.



Wei Han (S'16) received the B.Eng. degree from Northeastern University, Shenyang, China, in 2014, and the M.Eng. degree from The University of Hong Kong, Pokfulam, Hong Kong, in 2015, where he is currently working toward the Ph.D. degree in the Department of Electrical and Electronic Engineering.

His research interests include wireless power transfer techniques, power electronics, and renewable energies.



Wei Liu (S'17) received the B.Eng. and M.Eng. degrees from the College of Information and Control Engineering, China University of Petroleum (East China), Qingdao, China, in 2014 and 2017, respectively. He is currently working toward the Ph.D. degree in the Department of Electrical and Electronic Engineering, The University of Hong

Kong, Hong Kong, China.

His research interests include power electronics, wireless power transfer techniques, and electric vehicle technologies.



W. H. Lam (SM'09) was born in Hong Kong. He received the B.Sc. degree in computer and communication engineering from the University of Essex, U.K., in 1983, the M.Sc. degree in telecommunication engineering from the Imperial College, University of London, U.K., in 1984, and the Ph.D. degree from

the University of Southampton, U.K., in 1988.

From 1984 to 1988, he was sponsored by and collaborated with British Telecom Research Laboratory (BTRL), Plessey Research Laboratory (U.K.), and Bell Labs to work on the pan-European digital cellular mobile radio communications systems, which is then known as GSM. He was a member of the Mobile Radio Research Group and specialized in digital cellular mobile radio communications including GSM, CDMA, and RACE. In 1988, he joined STL (STC Laboratory), Harlow, U.K., where he was responsible for the UK DTI-LINK project “phones on the move” of DTI, micro-cellular project, formulation of the personal communication systems (PCN) architecture, and subsequently winning the operation license application of the British PCN. In 1989, he was with the Pan-European Digital Cellular Infrastructure R&D center, Motorola Limited, Swindon, U.K., where he was responsible for the development and validation of the GSM systems, radio resource network management project, which encompassed radio propagation measurements and prediction, geographical information systems (GIS), GSM and PCN radio

frequency planning, and radio network planning. In 1991, he joined the Department of Electrical and Electronic Engineering, University of Hong Kong. He has published more than 70 technical publications in the field of digital cellular mobile radio communications and the intelligent transport systems (ITS). He was the chairman and organizer of a series of regional conferences on mobile radio communications and a distinguished speaker and chairperson at several international conferences and meetings. His current research interest includes the next generation digital mobile radio and spread spectrum communications systems, ITS, power electronics and drives.

Dr. Lam received the SERC CASE award from the University of Southampton.